npj | materials degradation

Article

Published in partnership with CSCP and USTB

https://doi.org/10.1038/s41529-024-00510-5

The influence of recycling on the localized corrosion susceptibility of extruded AA6063 alloys

Salil Sainis ✉, Dan Persson, Karin Törne, Johan Tidblad & Dominique Thierry

An approach involving the quantification of microstructure characterized by different techniques such as SEM, EDS, and SKPFM is statistically treated to provide a deeper insight into the influence of recycling AA6063 on localized corrosion susceptibility. Particularly, the intermetallic particles and the two forms of localized corrosion – pitting and intergranular corrosion are systematically documented, measured, and analyzed. Even trace amounts of Cu and Zn introduced into the alloy from recycling had a remarkable effect on the localized corrosion susceptibility. The study found that the initiation and early evolution of the two localized corrosions are in competition, and the predominance of one over the other is closely linked to the composition of the alloy, and microstructure. Recycled variants with higher trace Cu made the alloy more susceptible to pitting attack whereas higher trace Zn is linked with greater IGC susceptibility. The trace amount of higher Zn addition has a particularly beneficial effect on pitting susceptibility as it reduces the likelihood of pitting even in alloys with a higher trace Cu content. The SKPFM results obtained in this study provided a basis for the circumferential pitting susceptibility around intermetallic particles, as a higher volta potential difference (ΔV) implied a higher driving force for corrosion. ΔV differences between the different variants were further explained based on trace recycled element distribution in the microstructure.

Aluminum and its alloys have been widely recognized for their physical properties such as high-strength-to-weight ratio, good formability making them materials of choice for a myriad of applications, notably in the automotive sector[1]. An additional benefit to using aluminum alloys is that they are highly recyclable[2]. As the demand for sustainability intensifies, aluminum stands out as a circular material that can be recycled multiple times without significant degradation of its intrinsic properties. However, the recycling process is not devoid of challenges. There is significant effort being made to better understand how scrap-related alloying elements affect the properties of secondary alloys to better design alloys and components in tolerance limits that make them economical while not deteriorating the properties[2]. Corrosion resistance is one such property that is crucial for the long-term durability of the material, another aspect that increases its sustainability.

The material under scrutiny in this research is AA6063 alloy with Mn, Si, Fe, and Mg in its composition. It is the material of choice in the automotive industry requiring extruded components due to its superior ductility and high strength[3]. Like in other aluminum alloys, AA6063 is susceptible to localized corrosion particularly pitting[4–6] and intergranular attack[7–11]. Both these forms of localized corrosion are due to heterogeneity in the microstructure[12]. Pitting occurs in the periphery of a cathodic intermetallic (IM) particle due to electrochemically different characteristic compared to the Al matrix[13]. An anodic dissolution of Al results in the formation of trenches around the cathodic IM[14–20]. Intermetallic particles like α-phase Al-Si-Mn-Fe accelerate pitting corrosion[11] as they are relatively cathodic with respect to the aluminum matrix in which they are present[21]. Intergranular corrosion (IGC) is similarly driven by potential differences, typically at grain boundaries due to the partitioning of elements during grain growth[10]. Both forms of localized corrosion are detrimental to the surface appearance and mechanical integrity as these localized corrosion damages are often the hot spots for fatigue cracks that can eventually lead to early failure of the component. Pitting corrosion has been shown to have a strong effect on the fatigue life of several aluminum alloys[4,22–25] including AA6063[26] which is under scrutiny in this work.

Cu additions to Al-Si-Mn-Fe alloys are made either deliberately[27] or can be introduced as an impurity from the recycling process[7] which can improve the mechanical properties but have significantly detrimental effects on the corrosion resistance[7,20,28]. Zn similarly has a deleterious effect on corrosion resistance[29]. Recycling of alloys can introduce alloying elements like Cu and Zn[30], which may not have been present in the

RISE Research Institutes of Sweden AB - RISE Corrosion, Kista, Sweden. ✉e-mail: Salil.sainis@ri.se

composition of primary AA6xxx and these affect the corrosion properties of the alloy.

Introduction of trace amounts of Cu negatively affects the IGC sensitivity because Cu segregates at grain boundaries due to its low solubility in aluminum solid solution (room temperature Cu solubility in Al is 0.02 at.%)[31]. Works of Kairy et al. [32–35] have provided significant insight into grain boundaries and the mechanism of IGC. These studies found a thin layer of Cu (~2 nm) along the grain boundary and precipitate-free zone in the region adjacent to the boundary. Due to differences in the chemical composition, especially Cu content, local cathodes[7–10] are formed that contribute to IGC[36]. Cu-rich IM particles form in 6xxx aluminum when Cu levels are relatively higher like the Q-phase IM[33,36], and because Cu-rich IM are highly cathodic[21] in nature, they make the alloys more susceptible to pitting attack. Zn has relatively greater solubility in aluminum (0.85 at.%)[37] and a greater fraction of Zn is required to precipitate IM particles. Increased Zn content in AA6060 deteriorated its corrosion properties[29], but higher Zn-containing AA7xxx showed contradicting results. Lutz et al. [10] made an interesting observation that the Cu:Zn ratio mattered for corrosion properties. In high Zn-containing alloys, its detrimental effect is countered when simultaneously high Cu is present in the alloy. This effect was also observed by Yamaguchi[38] who used an alloy with high Cu and Zn levels. Alloys that have a greater fraction of Zn as compared to Cu are more susceptible to intergranular corrosion because enrichment of Zn in the grain boundaries makes them preferentially anodic relative to the cathodic matrix and thus preferentially undergo anodic dissolution due to Zn being more active than Al[39].

Considering that both pitting and IGC are forms of localized corrosion affected by chemical heterogeneities in the microstructure, Cu and Zn introduced from recycling, manifesting in different ways, can change the corrosion behavior. An investigation is thus conducted in this study wherein different local properties (physical, morphological, chemical, and electrochemical) of microstructure are characterized, quantified, and analyzed in relation to the quantification of localized corrosion damage. Instead of solely relying on standard corrosion measurement techniques such as Open Circuit Potential (OCP), Potentiodynamic Polarization (PP) or Electrochemical Impedance Spectroscopy (EIS), this work meticulously documents the initiation and evolution of both localized corrosion forms in a reference AA6063 wrought alloy and compares it with three different recycled compositions with different trace amounts of Cu and Zn to study their influence on the microstructure and corrosion behavior. To obtain various microstructural characteristics, advanced characterization tools like Scanning Electron Microscopy (SEM), Energy Dispersive X-ray Spectroscopy (EDS), and Scanning Kelvin Probe Force Microscopy (SKPFM) have been employed. SEM and EDS characterize the morphology and chemical composition of phases and have been widely used for corrosion investigations. SKPFM is a relatively upcoming technique and can characterize the volta potential of different phases – a metric for the driving force for localized corrosion[40–47]. Sufficiently large number of observations from each have been made to obtain quantitative data, whose acquisition was aided by different machine learning-based tools like Trainable Weka Segmentation[48] and SEM Particle Segmentation (Beta)[49] plugins of Fiji ImageJ[50]. A novel data-intensive approach involving the quantification of microstructure (intermetallic particle geometry, volta potential difference) and corrosion damage (likelihood of pitting and intergranular corrosion and extent of intergranular corrosion) is presented to investigate the impact of recycling on corrosion susceptibility.

Results

Open circuit potential and potentiodynamic polarization

Open circuit potential (OCP) and potentiodynamic polarization experiments are the most widely accepted techniques to measure the electrochemical stability and the rate of corrosion of aluminum alloys, respectively. This was performed in a 0.1 M NaCl solution and the results are shown in Fig. 1. The OCP follows a very stable horizontal trend (Fig. 1a) which is similar for the primary and three secondary alloys of this study. Furthermore, the anodic branches of the polarization curve (Fig. 1b) are nearly identical, indicating that the corrosion behavior is similar for the four variants of AA6063. This indicates a rather similar behavior for all tested materials. The range of OCP values and potentiodynamic polarization curves are similar to those observed in other work[5].

Microstructure of the different variants of AA6063

This study focuses on the microstructures' effect on corrosion and in these interests, detailed microstructural characterization of the primary AA6603 alloy and the three secondary variants V1, V2, and V2 are described in this section. Figure 2a–d show respectively the microstructure of these alloys and they contain intermetallic (IM) particles (as indicated exemplarily in Fig. 2a). The intermetallic sizes in the microstructures of each of these alloys were measured using the SEM Particle Segmentation (Beta) plugin of Fiji ImageJ and a frequency distribution is presented in Fig. 2e. The particle size distribution appears to be nearly identical, and it is evident that recycling did not have any significant effect on the IM particle sizes.

The IM particles in the four variants of AA6063 were further characterized with SEM-EDS (Fig. 3a). The EDS maps shown here are qualitative showing only the distribution of elements Al, Si, Fe, Mn, Mg, Cu, and Zn in the microstructure of the four variants of AA6063. The particles were primarily found to contain Al, Si, Fe, and Mn, and further XRD characterization (not shown here) concluded that the IM phase in all these alloys is α-Al-(Fe, Mn)-Si phase. This α phase is commonly found in AA6063 alloys as shown in works by other researchers[3,11].

A quantitative analysis is also presented in Fig. 3b, c for deeper insight into the distribution of different elements within the IM particles. The quantitative analysis was performed on atomic fraction measurements with EDS over 20 different points over the IM in the microstructure of each of the four variants of AA6063. Nealy similar Fe, Si, Mn, and Mg are found from the many point EDS scans over IM (Fig. 3b), but the amount of Cu and Zn varied significantly as shown in Fig. 3c. Secondary alloy V1 (variant with a relatively higher trace amount of Cu and low Zn) showed much greater median atomic fraction of Cu as compared to primary alloy Ref. The other secondary alloy V2 which also had Cu introduced into it from recycling also showed greater median concentration of Cu in the IM. Cu has a low solubility in aluminum and so, a very small fraction of the Cu introduced from recycling can dissolve into matrix solid solution, the rest of the Cu goes into the IM as evidenced by Cao et al. [27]. Trace amount of Cu in the AA6063-T6 alloy studied by Örnek et al.[18], although added for increasing strength, was also found in the α-phase IM. The amount of Cu found in IM is statistically more spread in V1 and V2 as compared to the secondary variant V2. Zn content was also found to be higher in V2 and V2 than the nominal amount in Ref. To validate further that Cu and Zn were concentrated in the IM of recycled variants V1, V2 and V2, EDS point measurements over the aluminum matrix were also similarly statistically treated (Fig. 3d) and showed a different trend than the statistical analysis of EDS point scans over IM in Fig. 3c. Cu in an Al-Mn-Fe-Si alloy was found to dissolve partly in the Al matrix and partly in the α-phase IM particle[27]. The solubility of Cu in Al is much lower than that of Zn in Al, so the majority of Cu should go into the α-phase IM particle. The prevalence of more Cu in IM particles of relatively high trace Cu-containing recycled alloys V1 and V2 compared to Zn in IM particles (Fig. 3c) is thus justified.

Localized corrosion from immersion tests

After exposing different specimens of the same samples Ref, V1, V2, and V2 to 0.1 M NaCl solution for different times of 30 min, 2 h, and 24 h, differences in corrosion initiation and evolution were observed. In this study, two distinct corrosion morphologies have been observed and analyzed – namely pitting and intergranular corrosion (IGC). An exemplar of these two morphologies is shown in Fig. 4. The pitting corrosion observed here appears as a trench in the periphery of the α-IM particle, as observed and imaged also by Rynders et al. [14] IGC has a different morphology than pitting, wherein the damage follows the grain boundary profile and is a more severe form of localized corrosion compared to pitting.

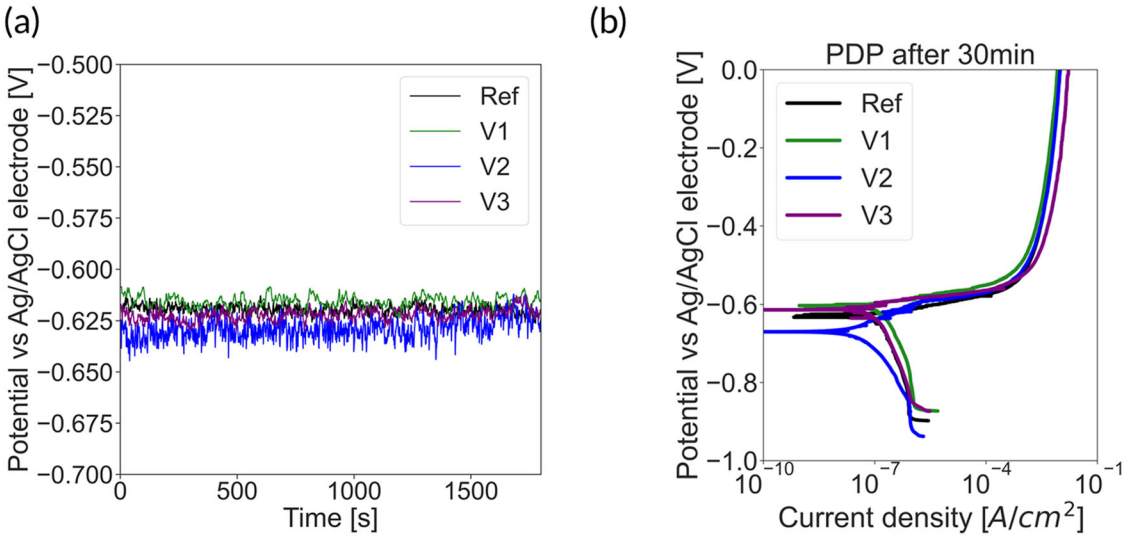

Fig. 1 | Electrochemical measurements performed on the four variants of AA6063 alloy investigated in the study. a OCP and **b** potentiodynamic polarization (PDP) measurement.

When the different variants were exposed to corrosive 0.1 M NaCl solution for a short time of 30 min, the differences in pitting are shown in Fig. 5 where green arrows indicate the absence of pitting and red arrows indicate the presence. While Ref, V2, and V2 did not show any discernible pitting corrosion damage after a short immersion time, secondary alloy variant V1 showed many more instances of pitting around IM. For investigating the evolution of pitting, micrographs of surfaces after 2 h and 24 h exposure are also presented in Fig. 5. It can be observed that all variants now showed pitting corrosion after medium-term exposure for 2 h. The V1 variant shows extensive corrosion product build-up over IM particles indicating that the extent of micro-galvanic coupling is much higher than others. After 24 h, the corrosion product build-up can also be seen over all IM in the other AA6063 variants, but the evolution of corrosion damage in Ref, V2, and V2 seems much slower than that for V1.

SEM-SEI micrographs taken at low magnification as seen in Fig. 6 show the IGC corrosion in the different alloy variants after exposure in 0.1 M NaCl solution for different times. The corrosion morphology here follows the grain boundaries as the attack profile seems to indicate. In certain micrographs like that of V1 and V2, corrosion product build-up over the IGC is also observed after 24 h exposure indicating that IGC damage was more aggressive in these relatively higher trace Cu-containing alloys.

Localized corrosion quantification

Figures 5 and 6 only provide qualitative evidence of pitting and IGC corrosion, respectively, and the microstructures were further analyzed quantitatively to arrive at the trends shown in Fig. 7. A representatively large number of IM (~600) were observed and manually accounted for pitting corrosion. The trends in the percentage number of IM showing localized pitting corrosion as a function of corrosive solution exposure is shown in Fig. 7a. At very short exposure time (30 min), <5% of IM showed pitting in Ref, V2, and V2 variants, but significantly more IM were susceptible to pitting (83%) for V1. After longer exposure of 2 h, the likelihood of an IM showing pitting corrosion was at comparable levels for Ref, V1, and V2 variants which increased to >95% likelihood after 24 h long exposure. V2 variant is an outlier with significantly lower proportion of IM showing pitting both at 2 h and 24 h long exposure. Since pitting in the form of trenching corrosion damage around an IM particle is of a probabilistic nature, the term "likelihood" signifies the fraction (in %) the number of IM particles that have shown clear trenching in SEM-characterized microstructures from all the IM observed after corrosion.

Two quantities, namely the number instances of IGC and the cumulative affected area with IGC, were measured with ImageJ and are shown in Fig. 7b. The total number of IGC initiation sites after short exposure of 0.5 h is comparable and the total corroded area was ~25000 μm^2 for all AA6063 variants. After 2 h exposure, the total IGC area and number instances for Ref alloy were comparable to those of the same variant for shorter 30 min exposure. Relatively, variants V1 and V2 showed greater area affected by IGC (~50000 μm^2) after 2 h exposure but V2 seemed to be most affected at >200000 μm^2. The total number of corroded sites after 2 h exposure decreased for recycled variants V1, V2, and V2 compared to total sites after 30 min corrosion, likely due to consolidation of IGC as the corrosion damage progresses. After 24 h exposure, IGC-affected area increased significantly in the case of V1 and V2, in V2 the levels were comparable high to those seen after 2 h exposure and the IGC-affected area for the Ref variant remained similarly low to that seen at shorter immersion times 30 min and 2 h.

It is interesting to note that, in the case of variant V2, pitting susceptibility was unusually low but IGC susceptibility unusually high after 2 h exposure. Since there are two localized corrosions competing for the O_2 required for the cathodic reduction reaction, one of the localized corrosion forms takes precedence and has to do with the extent of micro-galvanic coupling (MGC) reactivity. Higher Zn-containing alloys increase the intensity of MGC reactivity at grain boundaries and this makes it very susceptible to IGC. Whereas for the other higher trace Zn but also higher trace Cu-containing alloy, there is competition This variant has lower trace amount of Zn and higher trace amount of Cu, and given Zn's higher solubility in Al and being relatively more active, the IGC corrosion is significantly increased.

Volta potential characterization

The SKPFM technique was utilized to map the volta potential of polished surfaces of different AA6063 variants. Such measurements are performed in air but are considered a reliable measure of the corrosion potential[44] and cathodic breakdown potential[51] in aqueous solutions. Thus, the "strength" of the micro-galvanic couple can effectively be characterized by such a technique. Figure 8a shows the volta potential maps of the different AA6063 variants. A higher volta potential (indicated by brighter tone in the color bar) indicates that the local region is relatively cathodic.

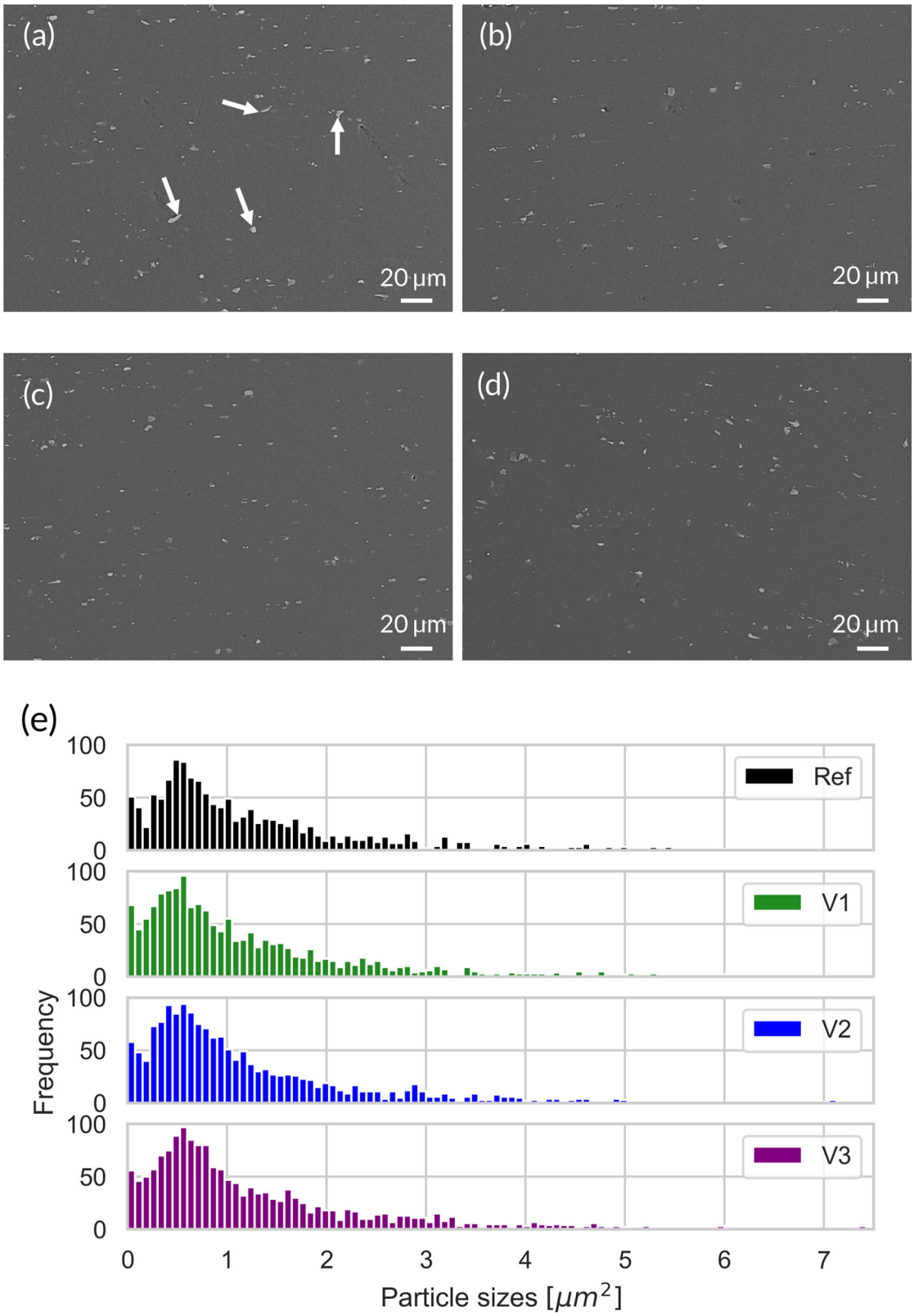

Fig. 2 | Microstructure and IM quantification of the four variants of AA6063 alloys. SEM-SEI characterized microstructure of **a** Ref **b** V1 **c** V2 and **d** V2 variants of the AA6063 alloy showing the IM particles and **e** particle size distribution.

Vice-versa, darker tones on the map indicate relative more anodic regions. The SKPFM mapping shows that the IM particles form a micro-galvanic couple with the matrix, the strength of which is determined from the difference between the volta potentials of the cathodic and anodic phases. A line scan across IM particles (indicated by the black arrow) yields a volta potential profile as plotted in Fig. 8b. Volta potential difference, or ΔV, is calculated from the difference between the volta potential of the α-phase IM (V_α) and the matrix (V_{Al}).

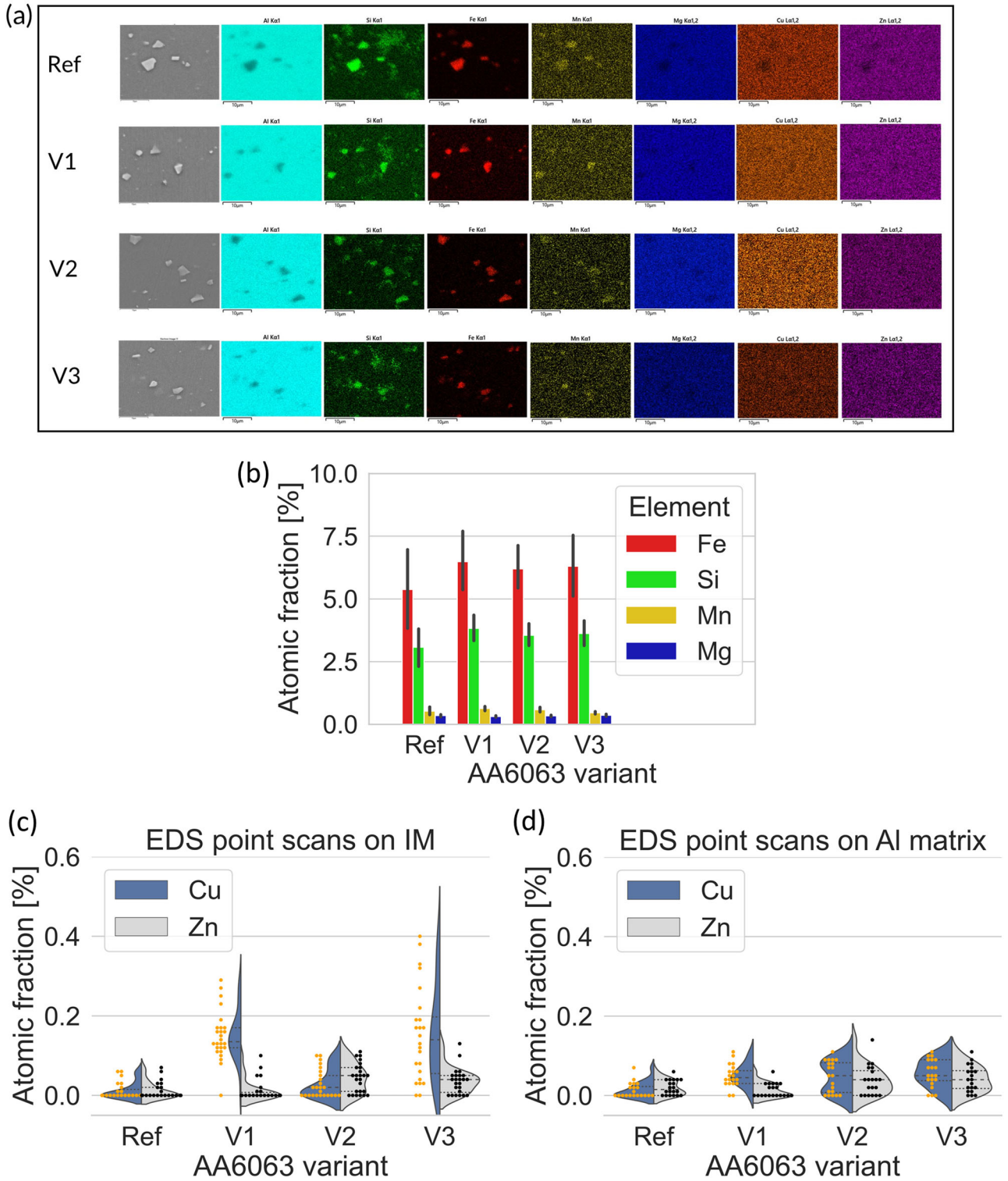

Fig. 3 | SEM-EDS characterized microstructure of the AA6063 variants. Qualitative and quantitative aspects showed through **a** elemental distribution map **b** atomic fraction of primary alloying elements Fe, Si, Mn, and Mg in the IM **c** violin plot showing the probability distribution of Cu and Zn in IM and **d** similar violin plot showing the probability distribution of Cu and Zn in Al matrix in the different variants of AA6063.

Typically, one measurement is not enough and so similar line scans and subsequent ΔV calculations were performed on all IM the SKPFM to get the distribution of volta potential differences of different IM in all the AA6063 variants (Fig. 9a). In comparison to Ref alloy, only V1 (high Cu, low Zn) showed higher median ΔV values. Comparatively, the ΔV values for V2 and V2 were nearly similar but lower than Ref. These observations are in line with localized corrosion experiments (Fig. 7a) wherein it was found that IM of only V1 alloy was more reactive than the Ref alloy. From this analysis, it is evident that IM in only those recycled alloys with higher trace Cu is more susceptible to pitting than primary Ref alloy. Higher trace Zn-containing alloy reduced the micro-galvanic couple effect and the pitting susceptibility. Zn has a beneficial effect on the pitting susceptibility even when the secondary alloy contains a higher trace Cu.

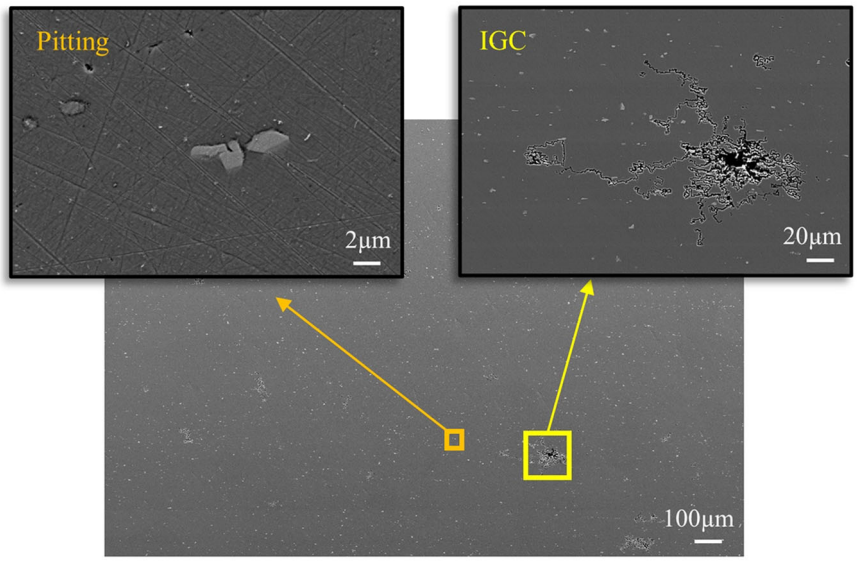

Fig. 4 | Exemplary low magnification SEM-SEI image showing the corroded surface after NaCl solution immersion and corresponding high magnification images showing the different corrosion attack morphologies – trenching and IGC.

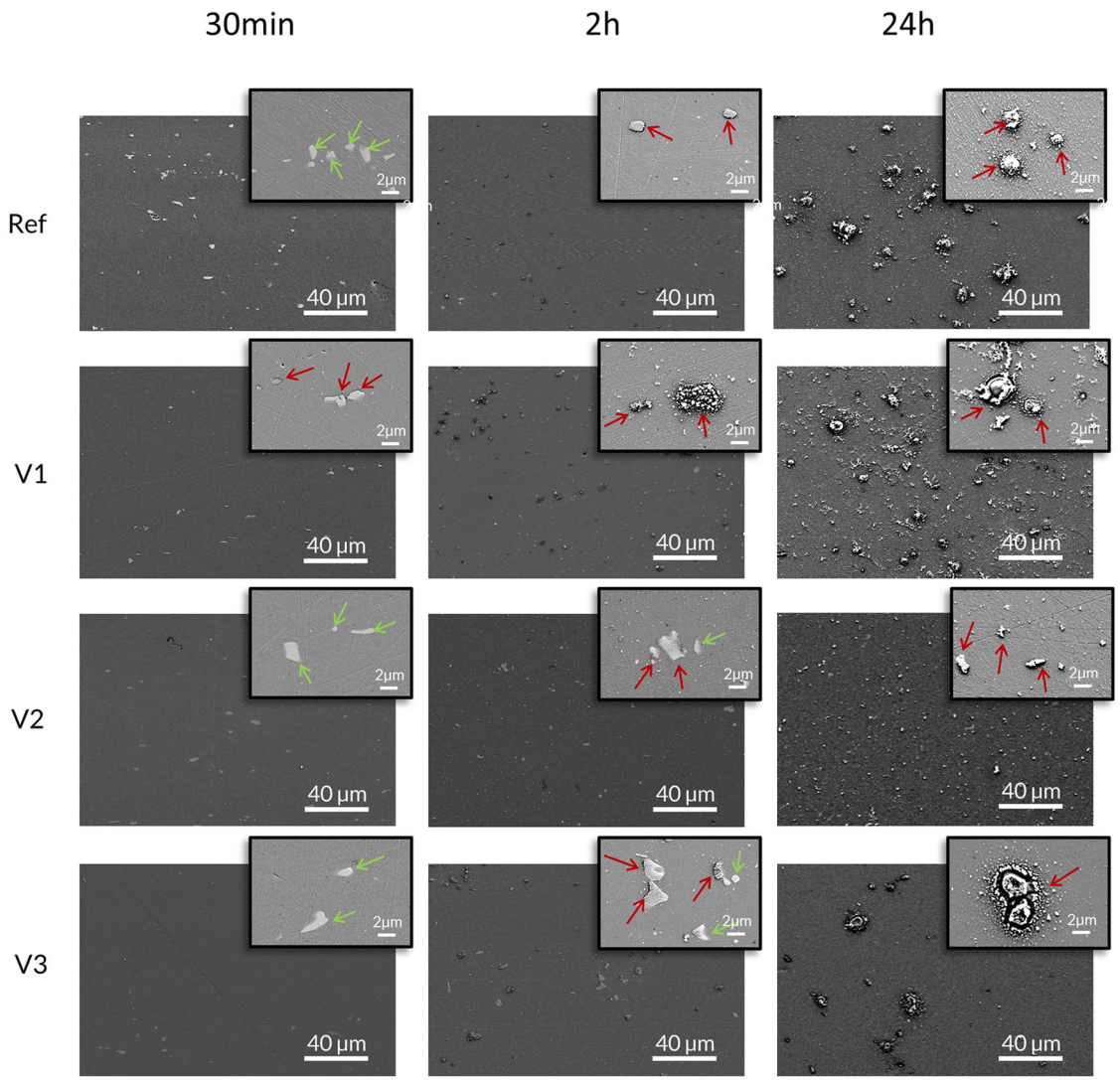

Fig. 5 | Matrix of SEM micrographs showing the corroded surfaces of the different AA6063 variants after exposure to 0.1 M NaCl solution for different times 30 min, 2 h, and 24 h. Insets of each micrograph shows a high magnification view of IM particles with green arrows indicating the absence of localized corrosion damage and red arrows indicating the presence of localized trenching corrosion.

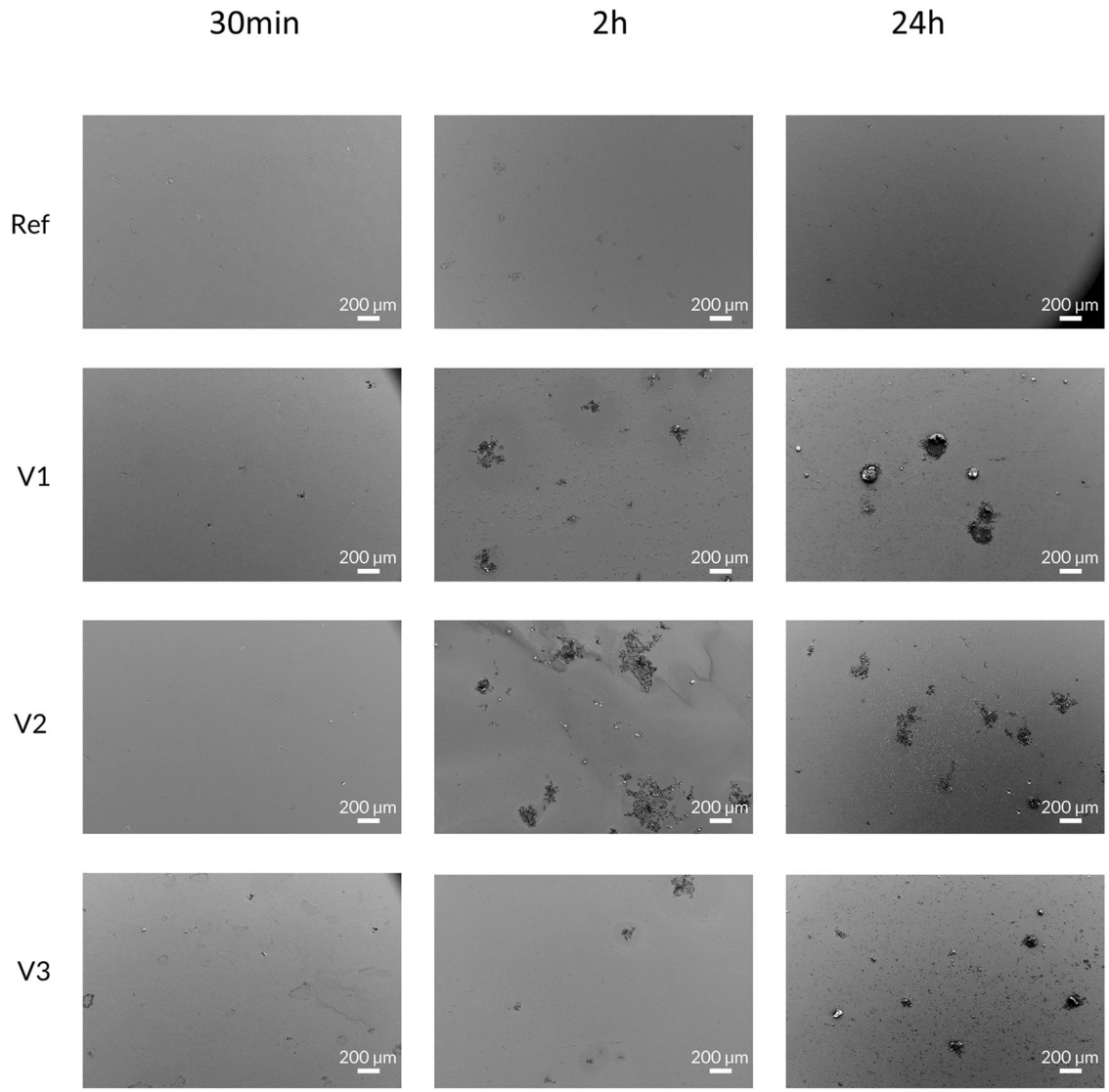

Fig. 6 | SEM-SEI image of the corroded surface showing the IGC attack on the different AA6063 variants after immersion in 0.1 M NaCl solution for different exposure times 30 min, 2 h, and 24 h.

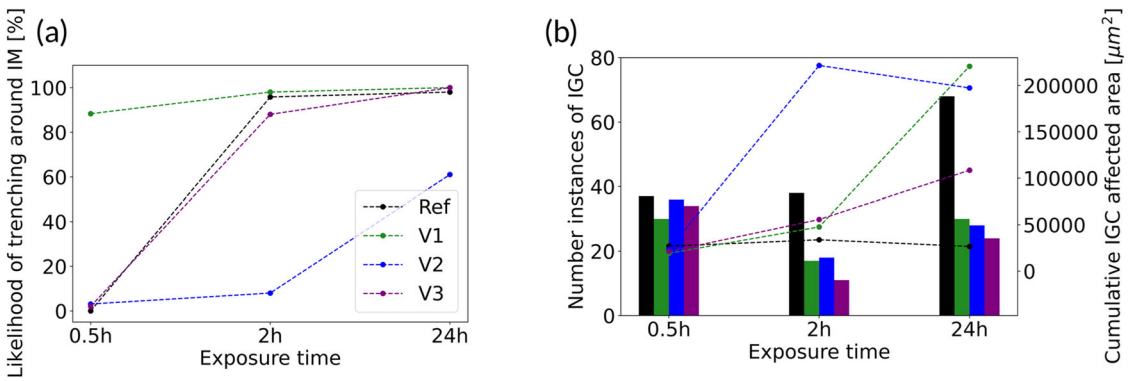

Fig. 7 | Quantitative analysis two different corrosion morphologies – pitting and IGC. They are represented as **a** Likelihood of pitting corrosion in the different AA6063 variants as a function of corrosive solution exposure time **b** Number instances of IGC observed (bar plot) and cumulative of affected area (dashed line plot).

The volta potential difference was also found to be also directly proportional to the IM size as shown in Fig. 9b. While in this study the particle size distributions were nearly identical for the recycled alloys as compared to Ref, discernable differences in the statistical distributions of ΔV were observed indicating a clear influence of trace elements on the volta potential of the particle. The size-volta potential correlation has also been reported in the work of Davoodi et al.[43] wherein they have also described its utility in designing corrosion-resistant alloys. In addition, we claim that trace amounts of Cu and Zn are also important.

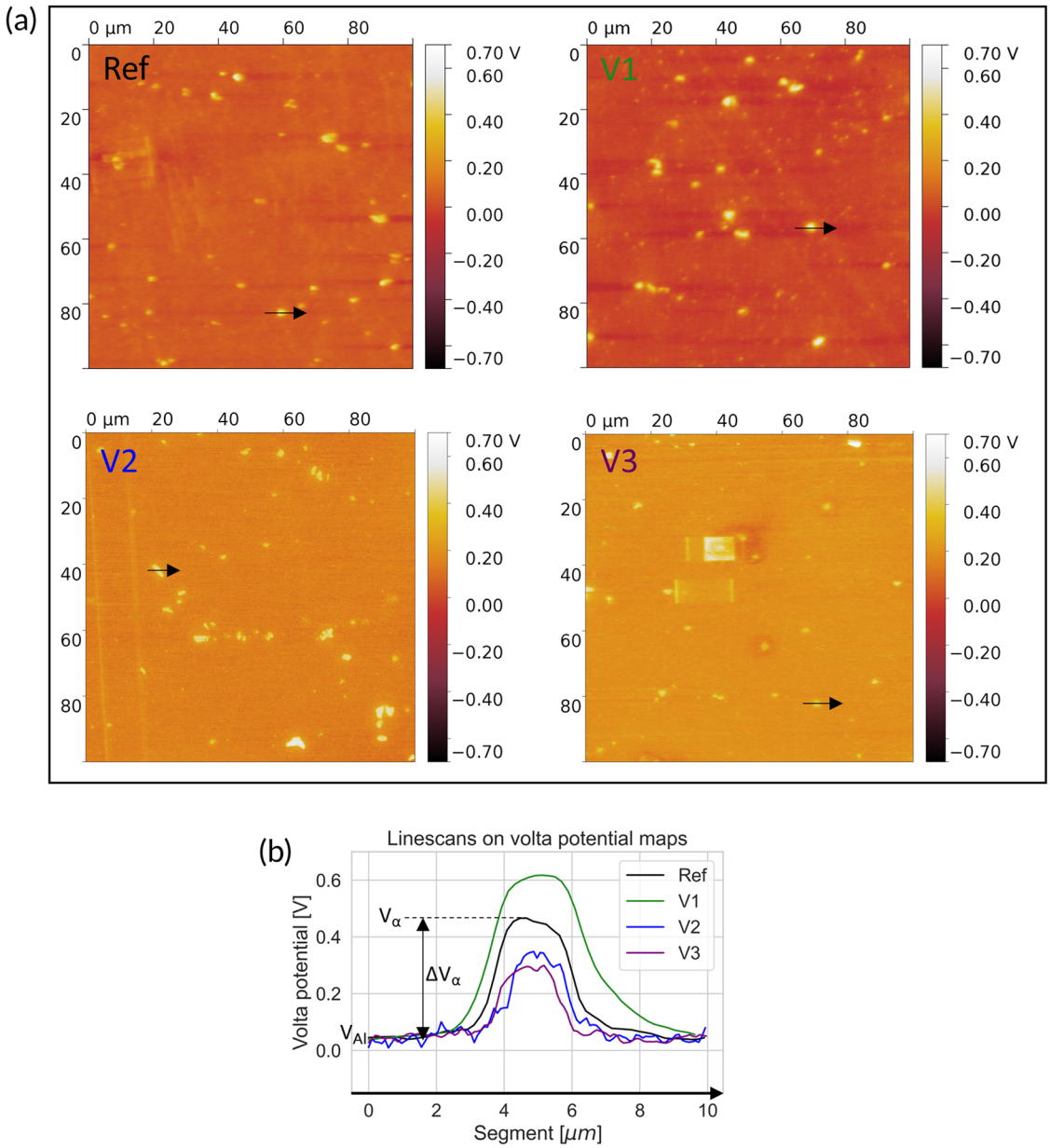

Fig. 8 | SKPFM characterization of the surface of different AA6063 variants. a Volta potential maps and **b** line profile of volta potential along the black arrows in the SKPFM maps.

Discussion

One primary and three secondary AA6063 variants investigated in this study had nominally the same type of α-Al-(Fe, Mn)-Si phase intermetallic particles in the microstructure, identified with SEM morphology and EDS composition. In all the variants, the particle size distributions of the IM were also found to be nearly identical. Despite the similar IM characteristics, significant differences in pitting corrosion initiation and evolution were found between the different variants. Furthermore, there were also differences in the IGC susceptibility. While pitting corrosion and IGC corrosion are principally similar, both starting at the local breakdown of the passive film, they follow different mechanisms of subsequent damage initiation and evolution. The microstructure has a key role to play in both localized corrosion forms and this study investigates the same with a data-intensive approach obtained from different characterization techniques. Furthermore, the recycling of aluminum alloys is a critical topic that needs to be investigated more to ensure increased use of sustainable materials for more demanding applications. So, in this section, we discuss some of the key findings on how the introduction of trace amounts of Cu and Zn (between 0.01 wt.% and 0.1 wt.%) from recycling processes may impact corrosion susceptibility.

The introduction of trace amounts of impurities Cu and Zn is compared with reference AA6063 alloy (<0.01 wt.% Cu and <0.01 wt.% Zn). Trace amounts of Cu and Zn in different ratios in the three recycled variants did not affect the general microstructure (in terms of the phases formed or their size distribution) and anodic polarization behavior after 30 min of OCP measurement, significant differences in pitting initiation and evolution were observed in this study. Cu and Zn get distributed in the different phases of the microstructure[35] which depends on their solubilities in the Al matrix. Cu has a significantly lower solubility in Al as compared to Zn in Al and so more Cu was found in the IM particle as compared to Zn. As a result, recycled variant V1 (0.1 wt.% Cu and 0.01 wt.% Zn) showed the greatest susceptibility to peripheral pitting attack showing high instances of pitting damage even after a short 0.5 h immersion. The

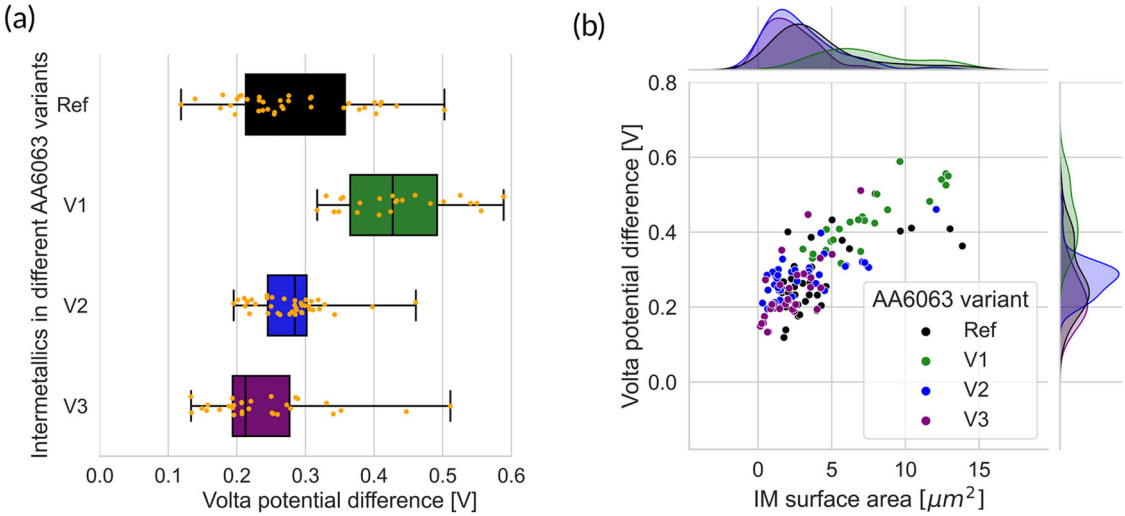

Fig. 9 | Quantitative observations from SKPFM characterization. Box and scatter plot showing the volta potential differences (ΔV) of the different IM in SKPFM maps of Fig. 7 (**a**) in the different AA6063 variants (**b**) Scatter and distribution plot showing a relation between the IM surface area and ΔV.

Table 1 | Composition of wrought AA6063 used in the study in Wt.%

Designation	Alloy	Si	Mg	Fe	Mn	Cu	Zn	Al
Ref	AA6063 ref	0.5	0.47	0.19	0.05	<0.01	<0.01	Balance
V1	AA6063 V1	0.53	0.48	0.2	0.05	0.10	0.01	Balance
V2	AA6063 V2	0.53	0.49	0.2	0.05	0.01	0.10	Balance
V3	AA6063 V3	0.52	0.48	0.2	0.05	0.10	0.10	Balance

recycled variant V2 (0.01 wt.% Cu and 0.1 wt.% Zn), on the other hand, had a lower trace amount of Cu but a higher trace amount of Zn and it showed lower susceptibility to pitting. It is worthwhile to note that trace Zn addition upon recycling had a beneficial effect on pitting in higher trace Cu-containing alloy variant.

The driving force for peripheral trenching around a cathodic IM particle is provided by volta potential differences between the cathodic particle and anodic matrix. In this study, we were able to correlate the volta potential observations with pitting susceptibility. Differences in the ratios of Cu and Zn are possibly the reason for differences in experimentally measured ΔV (Fig. 9a). Zn is more active than Al as it has a more negative potential, but Cu is very noble as it has a significantly more positive potential relative to Al. Segregation of Cu from solid solution into the IM would increase the ΔV.

Manual categorization and analysis of pitting likelihood, presented in Fig. 7a also show a trend that is explained based on ΔV (Fig. 9a). When recycling introduced only higher trace Cu, it partitioned into the IM particle and raised the ΔV to such high levels that significantly increased both the pitting likelihood and the extent of corrosion MGC reactivity, shown to be through large amount of corrosion build-up, even at medium-term exposure of 2 h. Comparatively, V2 alloy (0.01 wt.% Cu and 0.1 wt.% Zn) did not show such a heavy build-up of corrosion products on the IM particle.

Elevated trace amounts of Zn or Cu levels alone in AA6063 lead to greater susceptibility of intergranular corrosion, but together the effects are diminished as was observed in this study (Fig. 7b). High Cu content is said to precipitate Cu-rich compounds on the grain boundaries[7–9,32,34–36,52] due to its low solubility in Al and these Cu-rich sites on the grain boundaries preferentially act as local cathodes and promote the dissolution of Al at the grain boundaries. Very high cumulative IGC damage is thus observed (dashed green line in Fig. 7b) for high Cu-containing alloys after prolonged 24 h exposure as compared to Ref alloy. Similarly, high cumulative damage is also observed for a low Cu high Zn alloy (dashed blue line in Fig. 7b) and is attributed to more activity of Zn which segregates into grain boundaries and acts as preferential anodes, as explained by Stoknes et al.[39] Cu is said to counteract the negative effects of Zn when present together[10,38] as shown by the authors of the cited studies and the observations made in the current study agree with them. The recycled alloy containing high Cu high Zn has notably lower cumulative IGC damage (dashed purple line in Fig. 7b) as compared to other recycled compositions.

Methods

For the scope of this study, four distinct variants of the extruded AA6063 were investigated. These variants encompassed one primary alloy and three secondary alloys. The primary alloy, labeled "Ref" in this study is a wrought variant, whose composition is detailed in Table 1.

The three recycled aluminum alloys used in the study have the same base composition as the primary alloy but additionally contain different trace amounts of Cu and Zn. The recycled variant V1 contains trace amounts of relatively high Cu and low Zn, variant V2 contains relatively low Cu and high Zn and variant V2 has trace amounts of both high Cu and Zn. The amount of Cu and Zn in the recycled alloys were in between 0.01 and 0.1 wt.% and were varied in the three recycled compositions (designated as V1, V2, and V2), graphically illustrated in Fig. 10. High and low refers to lower and upper end of the range, respectively. The ratio of Cu:Zn in high Cu, high Zn variant V2 is close to 1:1. All the aluminum alloys used in this study were homogenized at 575 °C and then hot extruded into 4 mm thick flat profiles. The extruded sheets were quenched in water. No heat treatment has been performed on them.

Sample preparation

The alloys were cut into 1 cm × 1 cm square plates from large, extruded sheets of thickness 3 mm. They were subsequently embedded in a Buehler KonductoMet™ which is a conductive filled phenolic mounting compound.

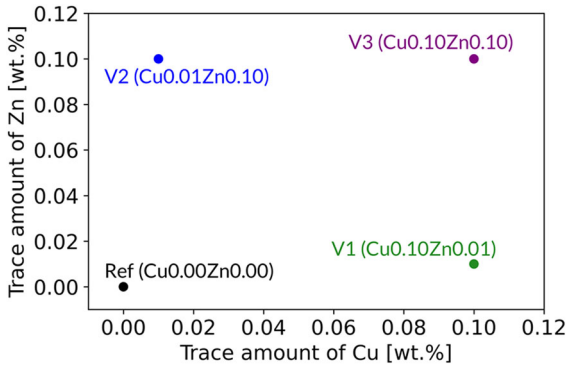

Fig. 10 | Graphical representation of the trace amounts of Cu and Zn in the primary alloy Ref and the three secondary alloys V1, V2, and V2.

The mounted specimens were ground with SiC abrasive papers and polished with different diamond suspension solutions of sizes up to 0.25 µm. Finally, the samples were rinsed with ethanol, dried, and stored in a desiccator for one day before subsequent corrosion experiments or surface analyses.

Corrosive solution exposure

To study the initiation and propagation of corrosion in the microstructure, separate polished samples from the four different alloy variants were immersed in a 0.1 M NaCl solution for different immersion times of 0.5 h, 2 h, and 18 h. After the immersion test, the samples were rinsed with deionized water followed by ethanol, and stored in a desiccator.

Structural, chemical, and surface characterization

Zeiss Gemini 300 scanning electron microscope (SEM) was the primary microstructure characterization tool used for observing the phases' morphology and corrosion damage. The micrographs in this manuscript were obtained in the secondary electron imaging (SEI) mode at 5 kV accelerating voltage.

The SEM is equipped with an Oxford Instruments Ultimax Energy Dispersive X-ray Spectrometer (EDS) for the chemical mapping and quantification of elements in the microstructure. The EDS results presented in this work were performed at an accelerating voltage of 20 kV. For both SEM and SEM-EDS characterizations probe currents were between 1 and 1.28 nA. EDS is a semi-qualitative characterization technique because the beam penetrates to a certain extent during probing (so-called interaction volume effect) and so highly accurate quantification of phases is not possible for bulk materials. In this work, a large enough dataset of quantitative results is statistically treated to explain distribution of different trace elements within the intermetallic phases. To ensure uniformity, point EDS data for all was obtained with the same parameters of 20 kV accelerating voltage and 90 s dwell time.

The electrochemical heterogeneity of the microstructure of different variants of polished AA6063 was characterized using a Park Systems NX10 Scanning Kelvin Probe Force Microscope (SKPFM) in the Electric Force Microscopy (EFM) mode using a NCSTAu tip with a tip radius of curvature <50 nm and resonant frequency of 160 kHz. The set point for the measurement was 9 nm and the tip was biased at 5 V.

Electrochemical characterization

Small coupons were cut from large extruded AA6063 sheets of the different wrought and recycled composition and polished up to 1 µm roughness and rinsed with deionized water and degreased with ethanol. The samples were then placed in a desiccator until characterization with PARSTAT 3000A-DX and a Gamry ECM8 Multiplexer potentiostat for the measurement of corrosion properties of the alloy 1 mm^2 area was exposed to a 0.1 M NaCl solution for 1800 s when the open circuit potential (OCP) was also recorded. The OCP remained stable after the 1800s monitoring. The samples were then subjected to potentiodynamic polarization in the anodic region. These tests were done using a 3-electrode setup where the samples were the working electrode, Pt wire the counter electrode and a saturated Ag/AgCl electrode was used the reference electrode. The scan rate for the measurement was 0.16 mV/s. The experiment for each alloy was repeated three times and the polarization plot reported here is the most representative one.

Image quantification analyses

Trainable Weka Segmentation plugin of Fiji ImageJ[50] was utilized for automatic classification of particles and corrosion damage which aided in the creation of binary phase images for easier quantifications. The quantification was further done on binary images with SEM Particle Segmentation (Beta) plugin[49]. The various microstructural data obtained were further statistically analyzed with a Python IDE called Spyder employing different statistical and data visualization libraries like Matplotlib[53] and Seaborn[54].

For the particle size distribution analysis, a total of 1811, 2013, 2131, and 2549 particles respectively from alloys Ref, V1, V2, and V2 particles were quantified microstructural area of 266750 $µm^2$ for each alloy. For pitting likelihood statistics, the 150 IM from each alloy were documented. For the IGC analysis presented in this paper, 10.75 million $µm^2$ area was scrutinized to gather statistics.

Data availability

Data will be made available upon reasonable request.

Received: 15 February 2024; Accepted: 2 September 2024;
Published online: 10 September 2024

References

1. Polmear, I. J. *Light Alloys.* From Tradit. Alloys Nanocrystals https://doi.org/10.1016/B978-0-7506-6371-7.X5000-2 (2005).
2. Raabe, D. et al. Making sustainable aluminum by recycling scrap: the science of "dirty" alloys. *Prog. Mater. Sci.* **128**, 100947 (2022).
3. Vazdirvanidis, A. et al. Examination of formability properties of 6063 alloy extruded profiles for the automotive industry. *Metals* **9**, 1080 (2019).
4. Rokhlin, S. I., Kim, J. Y., Nagy, H. & Zoofan, B. Effect of pitting corrosion on fatigue crack initiation and fatigue life. *Eng. Fract. Mech.* **62**, 425–444 (1999).
5. Zaid, B., Saidi, D., Benzaid, A. & Hadji, S. Effects of pH and chloride concentration on pitting corrosion of AA6061 aluminum alloy. *Corros. Sci.* **50**, 1841–1847 (2008).
6. Oliveira, M. U. et al. Manufacturing against corrosion: increasing materials performance by the combination of cold work and heat treatment for 6063 aluminium alloy. *Mater. Sci.* **26**, 30–33 (2020).
7. Bartawi, E. H. et al. The effect of trace level copper content on intergranular corrosion of extruded AA6082-T6 alloys. *Mater. Chem. Phys.* **309**, 128303 (2023).
8. Svenningsen, G., Larsen, M. H., Nordlien, J. H. & Nisancioglu, K. Effect of thermomechanical history on intergranular corrosion of extruded AlMgSi(Cu) model alloy. *Corros. Sci.* **48**, 3969–3987 (2006).
9. Svenningsen, G., Larsen, M. H., Walmsley, J. C., Nordlien, J. H. & Nisancioglu, K. Effect of artificial aging on intergranular corrosion of extruded AlMgSi alloy with small Cu content. *Corros. Sci.* **48**, 1528–1543 (2006).
10. Lutz, A. et al. Effect of Zn on the grain boundary precipitates and resulting alkaline etching of recycled Al-Mg-Si-Cu alloys. *J. Alloy. Compd.* **794**, 435–442 (2019).
11. Sekhar, A. P. & Das, D. Corrosion behavior of under-, peak-, and over-aged 6063 alloy: a comparative study. *Mater. Corros.* **70**, 2052–2063 (2019).
12. Zhang, W. & Frankel, G. S. Transitions between pitting and intergranular corrosion in AA2024. *Electrochim. Acta* **48**, 1193–1210 (2003).

13. Birbilis, N. & Buchheit, R. G. Electrochemical characteristics of intermetallic phases in aluminum alloys: an experimental survey and discussion. *J. Electrochem. Soc.* **152**, B140 (2005).
14. Rynders, R. M., Paik, C., Ke, R. & Alkire, R. C. Use of in situ atomic force microscopy to image corrosion at inclusions. *J. Electrochem. Soc.* **141**, 1439–1445 (1994).
15. Ji, Y., Mao, Y., Dang, L., Xia, D. H. & Hu, W. A high-resolution characterisation of localised corrosion of AA5083-H111 in simulated seawater by TEM. *Corros. Eng. Sci. Technol.* **58**, 223–229 (2023).
16. Peltier, F. & Thierry, D. Localised corrosion of intermetallic particles on aluminium AA2099-T8. *Corros. Eng. Sci. Technol.* **56**, 610–617 (2021).
17. Acosta, G. & Veleva, L. Mapping initial stages of localized corrosion of AA6061-T6 in diluted substitute ocean water by LEIS and SKP. *Rev. de. Metal.* **54**, e134–e134 (2018).
18. Örnek, C., Leygraf, C. & Pan, J. Real-time corrosion monitoring of aluminum alloy using scanning kelvin probe force microscopy. *J. Electrochem. Soc.* **167**, 081502 (2020).
19. Mallinson, C. F. et al. The localised corrosion associated with individual second phase particles in AA7075-T6: A study by SEM, EDX, AES, SKPFM and FIB-SEM. *Mater. Corros.* **68**, 748–763 (2017).
20. Kharitonov, D. S. et al. Corrosion of AD31 (AA6063) alloy in chloride-containing solutions. *Prot. Met. Phys. Chem. Surf.* **54**, 291–300 (2018).
21. Birbilis, N. & Buchheit, R. G. Investigation and discussion of characteristics for intermetallic phases common to aluminum alloys as a function of solution pH. *J. Electrochem. Soc.* **155**, C117 (2008).
22. Pidaparti, R. M. & Patel, R. R. Correlation between corrosion pits and stresses in Al alloys. *Mater. Lett.* **62**, 4497–4499 (2008).
23. Ishihara, S., Saka, S., Nan, Z. Y., Goshima, T. & Sunada, S. Prediction of corrosion fatigue lives of aluminium alloy on the basis of corrosion pit growth law. *Fatigue Fract. Eng. Mater. Struct.* **29**, 472–480 (2006).
24. van der Walde, K. & Hillberry, B. M. Characterization of pitting damage and prediction of remaining fatigue life. *Int. J. Fatigue* **30**, 106–118 (2008).
25. Ao, M., Liu, H., Dong, C., Feng, S. & Liu, J. Degradation mechanism of 6063 aluminium matrix composite reinforced with TiC and Al2O3 particles. *J. Alloy. Compd.* **859**, 157838 (2021).
26. Domínguez Almaraz, G. M., Ávila Ambriz, J. L. & Cadenas Calderón, E. Fatigue endurance and crack propagation under rotating bending fatigue tests on aluminum alloy AISI 6063-T5 with controlled corrosion attack. *Eng. Fract. Mech.* **93**, 119–131 (2012).
27. Cao, C. et al. Effects of Cu addition on the microstructure and properties of the Al–Mn–Fe–Si alloy. *J. Alloy. Compd.* **834**, 155175 (2020).
28. Zhan, H. et al. The influence of copper content on intergranular corrosion of model AlMgSi(Cu) alloys. *Mater. Corros.* **59**, 670–675 (2008).
29. Saito, T. et al. The effect of Zn on precipitation in Al–Mg–Si alloys. *Philos. Mag.* **94**, 2410–2425 (2014).
30. Das, S. K. Designing aluminum alloys for a recycling friendly world (n.d.) (accessed 6 October 2023); http://www.scientific.net.
31. Dirks, A. G. & van den Broek, J. J. θ-Al2Cu formation at room temperature in metastable Al□Cu alloy films. *Acta Metall.* **37**, 9–15 (1989).
32. Kairy, S. K. et al. Understanding the origins of intergranular corrosion in copper-containing Al-Mg-Si alloys. *Met. Mater. Trans. A Phys. Met. Mater. Sci.* **47**, 985–989 (2016).
33. Kairy, S. K., Rometsch, P. A., Davies, C. H. J. & Birbilis, N. On the electrochemical and quasi in situ corrosion response of the Q-phase (AlxCuyMgzSiw) intermetallic particle in 6xxx series aluminum alloys. *Corrosion* **73**, 87–99 (2017).
34. Kairy, S. K., Rometsch, P. A., Davies, C. H. J. & Birbilis, N. On the intergranular corrosion and hardness evolution of 6xxx series al alloys as a function of Si:Mg ratio, Cu content, and aging condition. *Corrosion* **73**, 1280–1295 (2017).
35. Kairy, S. K. et al. Exploring the electrochemistry of 6xxx series aluminium alloys as a function of Si to Mg ratio, Cu content, ageing conditions and microstructure. *Electrochim. Acta* **190**, 92–103 (2016).
36. Kumari, S., Wenner, S., Walmsley, J. C., Lunder, O. & Nisancioglu, K. Progress in understanding initiation of intergranular corrosion on AA6005 aluminum alloy with low copper content. *J. Electrochem. Soc.* **166**, C3114–C3123 (2019).
37. Skoko, Z., Popovic, S. & Stefanic, G. Microstructure of Al-Zn and Zn-Al alloys. *Croat. Chem. Acta* **82**, 405–419 (2009).
38. Yamaguchi, K. T. K. Effect of Zn addition on intergranular corrosion resistance of Al-Mg-Si-Cu alloys. In *Conference on Aluminium Alloys*, The Japan Institute of Light Metals. http://www.icaa-conference.net/ICAA6/index.html (1998).
39. Stoknes, M. Effect of copper and zinc on corrosion behaviour and mechanical properties in 6082-alloys. https://ntnuopen.ntnu.no/ntnu-xmlui/handle/11250/2377266 (2015).
40. Efaw, C. M. et al. Toward improving ambient Volta potential measurements with SKPFM for corrosion studies. *J. Electrochem. Soc.* **166**, C3018–C3027 (2019).
41. Örnek, C., Leygraf, C. & Pan, J. On the Volta potential measured by SKPFM – fundamental and practical aspects with relevance to corrosion science. *Corros. Eng. Sci. Technol.* **54**, 185–198 (2019).
42. Rahimi, E., Rafsanjani-Abbasi, A., Imani, A., Hosseinpour, S. & Davoodi, A. Correlation of surface Volta potential with galvanic corrosion initiation sites in solid-state welded Ti-Cu bimetal using AFM-SKPFM. *Corros. Sci.* **140**, 30–39 (2018).
43. Davoodi, A., Pan, J., Leygraf, C. & Norgren, S. The role of intermetallic particles in localized corrosion of an aluminum alloy studied by SKPFM and integrated AFM/SECM. *J. Electrochem. Soc.* **155**, C211 (2008).
44. Schmutz, P. & Frankel, G. S. Characterization of AA2024-T3 by scanning Kelvin probe force microscopy. *J. Electrochem. Soc.* **145**, 2285–2295 (1998).
45. Sainis, S. & Zanella, C. A localized study on the influence of surface preparation on the reactivity of cast Al-7Si-1Fe and Al-7Si-2Cu-1Fe alloys and their effect on cerium conversion coating deposition. *Appl. Surf. Sci.* **585**, 152730 (2022).
46. Sainis, S. & Zanella, C. A study of the localized ceria coating deposition on Fe-rich intermetallics in an AlSiFe cast alloy. *Materials* **14**, 3058 (2021).
47. Sainis, S., Roşoiu, S., Ghassemali, E. & Zanella, C. The role of microstructure and cathodic intermetallics in localised deposition mechanism of conversion compounds on Al (Si, Fe, Cu) alloy. *Surf. Coat. Technol.* **402**, 126502 (2020).
48. Arganda-Carreras, I. et al. Trainable Weka Segmentation: a machine learning tool for microscopy pixel classification. *Bioinformatics* **33**, 2424–2426 (2017).
49. Rühle, B., Krumrey, J. F. & Hodoroaba, V. D. Workflow towards automated segmentation of agglomerated, non-spherical particles from electron microscopy images using artificial neural networks. *Sci. Rep.* **11**, 1–10 (2021).
50. Schindelin, J. et al. Fiji: an open-source platform for biological-image analysis. *Nat. Methods* **9**, 676–682 (2012).
51. Andreatta, F., Lohrengel, M. M., Terryn, H. & De Wit, J. H. W. Electrochemical characterisation of aluminium AA7075-T6 and solution heat treated AA7075 using a micro-capillary cell. *Electrochim. Acta* **48**, 3239–3247 (2003).
52. Kumari, S., Wenner, S., Walmsley, J. C., Lunder, O. & Nisancioglu, K. Copper enriched by dealloying as external cathode in intergranular corrosion of aluminium alloy AA6005. *Corros. Sci.* **158**, 108090 (2019).
53. Hunter, J. D. Matplotlib: a 2D graphics environment. *Comput. Sci. Eng.* **9**, 90–95 (2007).
54. Waskom, M. L. seaborn: statistical data visualization. *J. Open Source Softw.* **6**, 3021 (2021).

Acknowledgements
The authors sincerely acknowledge the funding received from Vinnova, Sweden's Innovation Agency (Project ID: 2022-02952). We would like to thank Dr. Shilpa Kumari for the fruitful discussions.

Author contributions
S.S. performed all the experiments, treated and visualized the data. S.S., D.P., J.T., and D.T. were involved in the conceptualization and critical analysis. S.S. primarily wrote the manuscript and S.S., D.P., K.T., J.T. and D.T. were involved in revisions.

Competing interests
The authors declare no competing interests.

Additional information
Correspondence and requests for materials should be addressed to Salil Sainis.